

PAPER • OPEN ACCESS

Analysis of temperature distribution in PV-integrated electrochemical flow cells





To cite this article: Dorian Santander *et al* 2023 *Mater. Futures* **2** 045103

View the [article online](#) for updates and enhancements.

You may also like

- [A Zero-Dimensional Model for Electrochemical Behavior and Capacity Retention in Organic Flow Cells](#)
Sanat Modak and David G. Kwabi
- [Static charge outside chamber induces dielectric breakdown of solid-state nanopore membranes](#)
Kazuma Matsui, Yusuke Goto, Itaru Yanagi et al.
- [Comparative Electrochemical Analysis of Two Flow Cell Systems](#)
J. A. Goode, A. Ahmed, D. Pike et al.

Analysis of temperature distribution in PV-integrated electrochemical flow cells

Dorian Santander^{1,2} , Shaun Whitley^{1,3} , Jungmyung Kim¹  and Downon Bae^{1,*} 

¹ Institute of Mechanical, Process and Energy Engineering (IMPEE), School of Engineering and Physical Sciences, Heriot-Watt University, Edinburgh EH14 4AS, United Kingdom

² École nationale supérieure d'électricité et de mécanique de Nancy, Vandœuvre-lès-Nancy, France

E-mail: d.bae@hw.ac.uk

Received 6 June 2023, revised 26 July 2023

Accepted for publication 22 August 2023

Published 19 September 2023



CrossMark

Abstract

Photovoltaic (PV)-integrated flow cells for electrochemical energy conversion and storage underwent a huge development. The advantages of this type of integrated flow cell system include the simultaneous storage of solar energy into chemicals that can be readily utilized for generating electricity. However, most studies overlook the practical challenges arising from the inherent heat exposure and consequent overheating of the reactor under the sun. This work aims to predict the temperature profiles across PV-integrated electrochemical flow cells under light exposure conditions by introducing a computational fluid dynamics-based method. Furthermore, we discuss the effects of the flow channel block architecture on the temperature profile to provide insights and guidelines for the effective remedy of overheating.

Supplementary material for this article is available [online](#)

Keywords: solar redox flow battery, CFD, redox flow cell, energy conversion, temperature profile

1. Introduction

In recent years, photovoltaic (PV)-integrated electrochemical flow cells, such as solar rechargeable redox flow batteries (SRFBs), have been highlighted as a means of simultaneously storing solar energy into chemicals, which can be readily utilized to generate electricity *via* reversible reactions. In general, redox flow batteries (RFBs) are characterized by a low-levelized cost with a long cycle life with fast kinetics. Moreover, its power can be extended without the risk of fire simply by installing larger electrolyte storage tanks. Due to these advantages, intensive effort has been directed

into the development of efficient photoelectrodes and suitable redox electrolytes for SRFB applications, and some recent reports have made them promising candidates for renewable energy storage [1–4].

However, most studies overlook the practical challenges arising from the inherent thermal degradation of the photoelectrochemical redox kinetics. Some groups have claimed that it can be remedied by heat transfer into the electrolyte [5], but not much insightful in-depth analysis of the thermal impact on the SRFBs has been shown. Kamat *et al* demonstrated a temperature dependency of a photoelectrochemical cell using a stationary reactor with a TiO₂ photoanode for the O₂/OH[−] redox reaction in 1978 [6]. Since then, only few meaningful works have used practical flow cell reactors [7–9]. Although most studies have focused on the effects of temperature changes on the overall electrochemical performance, there have been only a few reports on the thermal regulation efficacy of the electrolyte.

As shown in our previous modeling work, the SRFB integrated with a c-Si solar PV system shows a voltage-loss rate

³ Current address: AECOM, Edinburgh EH3 5DA, United Kingdom.

* Author to whom any correspondence should be addressed.



Original content from this work may be used under the terms of the [Creative Commons Attribution 4.0 licence](#). Any further distribution of this work must maintain attribution to the author(s) and the title of the work, journal citation and DOI.

in the order of *ca.* 100 mV at a peak time of the day due to thermal recombination, resulting in a severe loss in solar-to-chemical conversion exceeding 20% compared to the ideal condition without any thermal loss [10]. Despite positive theoretical expectations, the recent dimensional fluidic modeling work using a model flow cell, which is similar to the state-of-the-art SRFB demonstrated by Li *et al* [3], exhibited an overheating of the photoelectrode under long-term heat exposure [11], implying the need of an advanced physical approach for a feasible thermal regulation of the system.

The working principle of the widely used flow cell architecture for the SRFB (figures 1(a) and (b)) is that the electrolyte flow, which is placed directly behind the photo device, absorbs light-induced charge carriers, whereas certain ions are transported to the counter electrode side via the ion exchange membrane (i.e., counter ion X in figure 1(c)) to complete the full redox reactions (i.e., reduction and oxidation) as shown in figure 1(c). The heat comes from the photo device side, and the temperature gradient between the outer surface of the device and electrolyte fluidic channels is the primary driving force of the heat transfer.

The aim of this paper is to predict the temperature profile across the redox flow cell integrated with a photo device under light exposure by introducing computational fluid dynamics (CFD) methods using ANSYS FLUENT. Furthermore, we aim to discuss the impact of the flow cell stack design on the temperature profiles to provide insights and guidelines for the development of a flow cell that can effectively remedy the thermal losses caused by the heat transfer to the electrolyte flow.

2. Methodology

2.1. Model development

Determining the structure and materials of the PV-integrated electrochemical flow cell is the first step for the theoretical modeling, and then the operating conditions and environmental considerations are followed. The model flow cell comprises a proton exchange membrane, porous carbon felts, a graphite block with flow channels, and a photo device mounted on the graphite block (i.e., zero gap design). These components are assembled in a stack (figure 1). It is worth noting that the stack in figure 1 represents the solar charging component of the dual-cell-based solar-rechargeable electrochemical flow cell system [12], and the analysis of the flow cell component for the electricity generation is beyond the scope of this work.

2.2. Model description

The flow field consists of vertically symmetric flow channels and electrodes (figure 1(a)). The inlet channel of the flow field acts as the flow path where the electrolyte fluid has a direct interface with the carbon electrode and graphite block. The inlet channel is an S-shaped serpentine, and the electrolyte flow rate is assumed to be uniform across the flow channel. The plane viewing area of the flow cell unit is 25 cm² for the

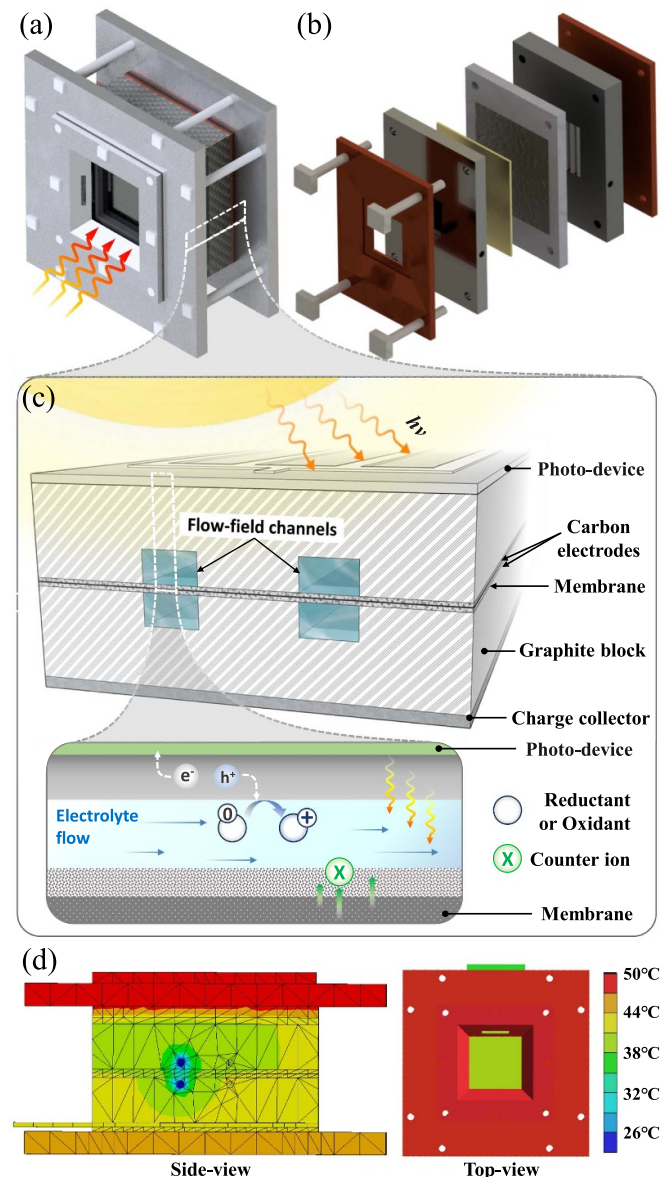


Figure 1. (a) Physical model of the PV-integrated electrochemical flow cell and (b) the scheme of the flow cell setup showing the main components of the device. (c) Schematic diagram of the cross-section of the flow cell configuration illustrating the vertical heat and charge transfers across the flow cell under the light exposure and (d) their computational analysis of temperature profile across the flow cell under 1 sun condition.

expanded model study in figure 1(d). Because the SRFB operates under sunlight, the photo device side is exposed to the air; therefore, both convective and radiative heat transfers at the air/solid boundary will be applied, whereas the conduction transfer mode occurs between the solid/solid boundaries (e.g., PV and carbon blocks).

In general, a 20% efficiency crystalline silicon-based photo-device (c-Si) produces *ca.* 35 mA cm⁻² under the full spectrum 1-sun condition [13], and this current flows through the graphite block, generating heat of j^2Rt (j —current density, R —resistance, t —time) during the photocharging reaction, that is, the unused absorbed solar energy is transferred in

the form of heat at the maximum conversion efficiency condition, and the current-induced heat passes through the graphite block from the photo device. At the same time, part of the heat is transferred back to the air side (i.e., heat loss, Q_{loss}) [14]. As described earlier, this work aims to predict the flow cell's temperature profile under heat exposure conditions, considering the heat balance between the transferred heat to the flow cell and the Q_{loss} for the cases under idle and photocharging conditions. The heat balance approach allows radiative and convective heat fluxes between the components to figure out the temperature conditions described elsewhere [10, 14]. It is also worth noting that external exchanges occur between the flow cell reactor and the air side on top of the reactor. Heat transfer between external environments other than the top air side has not been considered.

The CFD simulations are performed using two models which aim to highlight the effect of three different aspects: (i) the flow rate of the electrolyte, (ii) the graphite block thicknesses, and (iii) the flow channel shape, which is the first model used is an SRFB with two straight flow channels on each side of the membrane. The second one comprises two S-shaped serpentine flow channels with variable graphite thicknesses to explore the impact on the larger area.

For the dimensional analysis using CFD studies, we imitate a commercial lab-scale flow cell reactor structure with an operational area of 25 cm² (from Redox-flow.com) used in our laboratory. It is also worth noting that, except for figure 1, the modeling study only applies to the active area, meaning that the holding structure, such as the end plate, is not considered as it does not affect the heat transfer. As shown in figure 1(d), most of the heat is absorbed by the metallic frame (red-colored), leading to undesired heat transfer from the photo device to the frame.

2.3. Material parameters of a CFD model

The PV-integrated electrochemical flow cell models considered for the simulations in this paper consist of generally used components. The dimensional information used for both models is listed in table 1. Again, the model is only developed on the active structure, meaning that the holding structure is not considered as it does not affect heat transfer.

2.4. Design of CFD boundary conditions

Some assumptions have been made to simplify the model. For instance, the cross-contamination and diffusion of electrolytes across the porous carbon felt and the membrane are neglected, and the simulations are based on steady-state and non-isotherm evolution. The fluid is also considered incompressible and the FLUENT solver considers the Reynolds number related to the flow of water in the channel, whose value reflects a turbulent flow (higher than 10⁴) and general fluidic properties of the electrolyte considered in the channel are supposed to follow those for the water. Due to the high Reynolds number and low complex fluidic exchange, the turbulent model $k-\epsilon$ was selected [18]. Indeed, the simulation aims to analyze the heat exchange in each solid part of

Table 1. Thermal properties and thicknesses of the solar charging flow cell components used for the modelling works [10, 15–17].

Type of layer	Thermal conductivity (W m ⁻¹ ·K)	Thickness
Membrane (Nafion NM 117)	0.67	183 mm
Graphite felt (Sigratherm GFA5)	0.06	0.2–3 cm
Carbon felt (SIGRACET® AA)	<0.3	280 mm
Current collector	16	2 mm
TiO ₂ protective layer	4.8–11.8	50 mm
Pt catalytic layer	77.8	5 nm
c-Si device	148	150 μm
EVA protection film	0.23	75 mm
Glass cover	1.8	3 mm

the structure. With the fluidic channel structure being symmetrical and not complex, the $k-\epsilon$ turbulent model is suitable, with good convergence and the required low capacity calculation [19]. The temperature of the electrolyte in the inlet flow channel is set to be at the ambient temperature of 20 °C. Indeed, for the recirculation model, the heating of the fluid is not considered outside the battery. In addition, no effect from chemical or electrochemical reactions is considered for the combined fluid-thermal simulations studied in this work. The fluid flow through the porous carbon felt is also modeled considering the viscous and inertial resistance determination using the absolute permeability of the material, such as carbon felt from Sigracet [19–21] with the mean pore diameter of 42–44 μm and a uniform open porosity of 0.89 [21]. To save the computing time, the meshing is refined in the region in direct contact with the flow channels (the graphite layer and the carbon felt layer) as well as near the area, implying a modification of the thermal transfer due to structural variation as at each contact point between the different layers. Indeed, the mesh sizing is reduced from 5 mm to 2.5 mm. It is based on a hexagonal mesh in the majority and a tetragonal one due to the size element refinement. To ensure the quality of the meshing, the evaluation was based on the skewness and the orthogonal quality mesh spectrum equal to 0.009 and 0.98, respectively. It is noteworthy that the optimal skewness is equal to 0, and the optimal orthogonality is equal to 1.

The temperature of the SRFB structure is initially assumed to be at the ambient value of 20 °C. A zero heat flux, describing adiabatic conditions, is set for the walls of the structure, except for the top face (i.e., the photo device) and the lower face (i.e., current collector), meaning the heat cannot be transferred through the lateral faces. The electrolyte flow rate is varied from 1 to 70 ml min⁻¹ according to previously published works [9, 13, 14]. As described elsewhere, the capacity and energy density of RFBs are closely related to the flow rate [22]. Unlike conventional RFBs, the operating characteristics of SRFBs during the charging process differ from

the well-known RFBs. For instance, solar redox flow cells with metal oxide photo devices show a quite low photocurrent of $1\text{--}2\text{ mA cm}^{-2}$ [23], and the silicon-based flow cell showed a level of ca. 30 mA cm^{-2} [1], implying the solar RFB can operate at flow conditions lower than those required for typical RFB systems.

The objective of these simulations is to analyze the influence of the atmosphere, electrolyte temperature, and graphite thickness on the temperature profile of the solar charging compartment of the SRFB using the model reactor and CFD studies described earlier. The heat production by the Joule effect corresponding to the phenomenon of electricity production in the c-Si solar PV system is fixed for all the simulations, considering a photocurrent of 35 mA cm^{-2} and a surface resistance of $10\ \Omega\text{ cm}^2$ [13].

3. Results and discussion

To assess the temperature distribution of a PV-integrated RFB earlier described, two models of graphite blocks with various thicknesses (20, 10 and 2 mm) are used. For both models, upstream simulations have presented that a more efficient and homogeneous cooling system can be achieved by placing fluid inlets and outlets on either side of the battery, opposite to each other, as shown in figure 2. The variation of the temperature is applied on the top of the solar cell, representing the ambient solar radiation received by the battery and the thermal heat produced by the internal reaction during the electricity generation process.

3.1. Model 1: straight flow channel

For all case studies, the surface of the PV cell on the top of the flow cell is exposed to heated air conditions during the summer season according to previous theoretical studies [9, 15], representing the ambient solar radiation received by the solar charging component during the solar charging process. As described earlier, Model 1 considers two straight flow channels on each side of the membrane, illustrated in figure 2.

The first parameter to study the temperature profile change across the flow cell is the flow rate of the electrolyte at a fixed thickness of the carbon flow field block. Figure 3 shows the temperature profile across the solar rechargeable flow cell comprising 20-mm-thick graphite blocks (20/20 mm each), as well as with flow channels and solar cells mounted on top of the upper block performed for a range of flow rates with the respective thicknesses of 10 mm and 2 mm. It clearly shows that the flow rates chosen cannot regulate the surface temperature of the solar charging component for the first two thicknesses, showing that the overheated outermost layer (PV cell surface) with the temperature ca. $60\text{ }^\circ\text{C}$. Increased flow rates at 70 ml min^{-1} had also been simulated as well; however, no significant change in the upper cell's temperature was observed (figure S1; supplementary information). The overheating of the block is more obvious for the flow rates below 5 ml min^{-1} . The temperature profile within the electrolyte channels also significantly increases, which may lead to

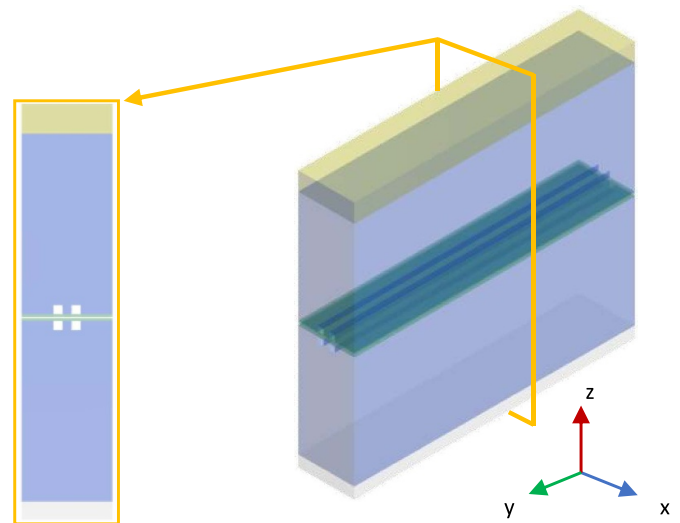


Figure 2. Cross-sectional view of the first model of PV-integrated redox flow battery considering straight flow channels as an electrolyte exchange structure.

unwanted redox chemical degradation, precipitation [10, 24, 25], or redox potential shifts as described elsewhere [26, 27].

Figure 3 also depicts two other graphite thicknesses (10 mm and 2 mm) with the same flow rate range assessed. The temperature profile of the 10-mm case is quite similar to the 20-mm case. However, the 2-mm-thick graphite shows an interesting result that the light-illuminated surface temperature can be regulated, dragging the PV surface temperature down to ca. $40\text{ }^\circ\text{C}$, implying that the amount of energy stored in the thinned carbon block is relatively low and thus can be dissipated by the fluid more easily. One possible solution to mitigate the above-described overheating effect is to minimize the graphite thickness. Indeed, the model system with a thick graphite block has a higher heat energy storage capacity, and thus, the transferred heat is more difficult to dissipate by the fluidic electrolyte. Because the thickness of the graphite block and its heat storage capacity are proportional, a high-temperature profile appears in the 20-mm block. These relatively high-temperature conditions exert a detrimental effect on the performance degradation of solar components. The ionic conductivity of the redox electrolyte can be improved at an elevated temperature [28]. The viscosity of the electrolyte decreases with the temperature due to lower molecular interactions and an easier mass transfer [29], but at the same time, shifted redox potential and cell voltage can lead to decreased power of the system.

Furthermore, the solubility of the redox couples directly as a function of the temperature. Organic electrolytes, for example, quinone/hydroquinone redox couple (AQDS) families have limited solubility in aqueous media (less than 1 M [30]), and this can be increased at an increased temperature [31]. In the case of irreversible precipitation formation due to the solubility limit, it will decrease the concentration of the active substance and impedes the electrolyte flow across the porous electrode [32].

Another interesting feature is the gradual heating of the electrolyte fluid inside the channels at low flow rates (e.g.

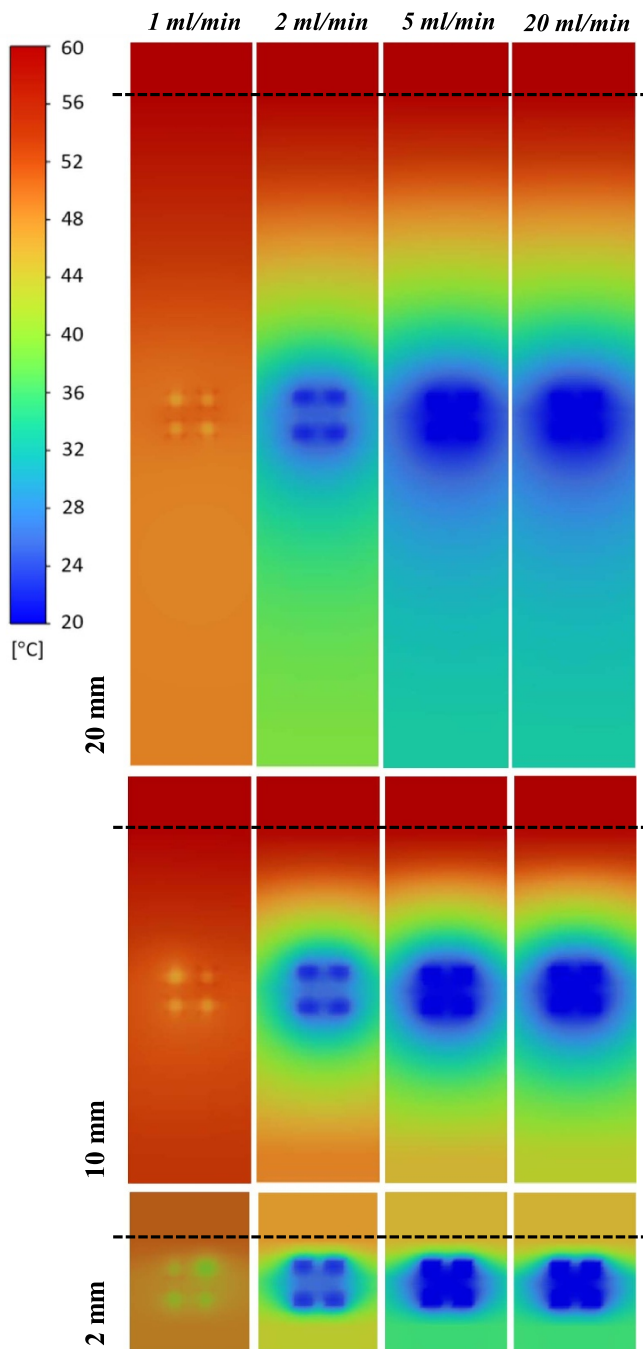


Figure 3. Temperature profile for a range of flow rates (1, 2, 5, 20 ml min⁻¹), for different graphite thicknesses of 20 mm, 10 mm, and 2 mm. The dash line represents the limit glass-covered photodevice/graphite block interface.

under 2 ml min⁻¹), as shown in figure 4(a). The heat received and produced by the solar component passes through the different layers of the battery until it comes in contact with the top electrolyte fluid, where a heat exchange will take place. This heat will be absorbed by the fluid along the flow channels, which will increase the temperature of the fluidic electrolyte. The bottom flow channel reacts similarly, exchanging heat with the top one to compensate for the temperature increase. However, for flow rates lower than 5 ml min⁻¹,

the fluidic structure will not be able to compensate for this temperature increase.

In contrast, this result implies that this overheating phenomenon in the flow cell can be exploited in reverse for heat-driven electrochemical energy storage technologies, such as thermally regenerative electrochemical cycle (TREC) and thermoelectrochemical cells (TEC), where the redox potential gradient at different temperatures is the main driving force for the operation [33, 34].

3.2. Model 2: serpentine structure channel

In our first set of simulations, the solar redox flow cell's sensitivity to heat exposure was evaluated under two variables, that is the graphite and the flow rate. However, there are apparent limitations to practical applications, considering the flow fields of the existing RFBs. While previous analyses assumed a linear fluidic channel model, most state-of-the-art SRFBs have a single passage of a serpentine flow channel. Parallel linear flow fields are quite common just because they are easy to manufacture. Although the previous model in figure 3 reflects the local temperature variation, using two straight flow channels on each side of the flow cells, figure 4(b) demonstrates the temperature profiles across the cross-section with a serpentine electrolyte flow channel, covering the whole interface between the graphite blocks. We note that the serpentine structure consists of 24 straight flow channels connected to each other.

Assuming that the graphite block with a serpentine flow channel structure has a thickness of 2 mm, as it can be seen in figure 4(b), using a serpentine structure leads to better results on the temperature profile with a much lower solar cell and top block's temperature compared to the first model. However, this is not valid for a flow rate lower than 5 ml min⁻¹. Interestingly, figure 4(b) shows that for a flow rate below 2 ml min⁻¹, the fluidic electrolyte is not able to cool down the solar cell sufficiently. Moreover, the electrolyte flow channel is also heated up, leading to the temperature of the local flow channel in the middle of the blocks up to 60 °C. Unlike the previous model, the fluid exchange energy over a much larger pathway, corresponding to a higher amount of transferred energy from the top block than the previous model in figure 4(a). For instance, it heats up more easily for even higher flow rates. In figures 4(b) and 5, the temperature of the fluid at the end of the channel is higher than the temperature of the solar cell at that moment. In the same way, as Ahadi *et al* demonstrated, the accumulation of energy leads locally to a significant increase in the temperature being maximum [35].

By taking a closer look at the temperature profile in the channels, as we did for model 1, it can be seen that an additional mechanism takes place for the second model highlighted in figures 4(b) and 5. The fluid in the bottom flow channel partly dissipates the energy accumulated in the fluid in the upper block. Obviously, the temperature of the top fluid is then cooled down when approaching the end of the channel (outlet), where the inlet of the bottom flow channel is placed. The bottom flow channel is not directly in contact with the top graphite block; however, especially for a flow rate below 5 ml min⁻¹,

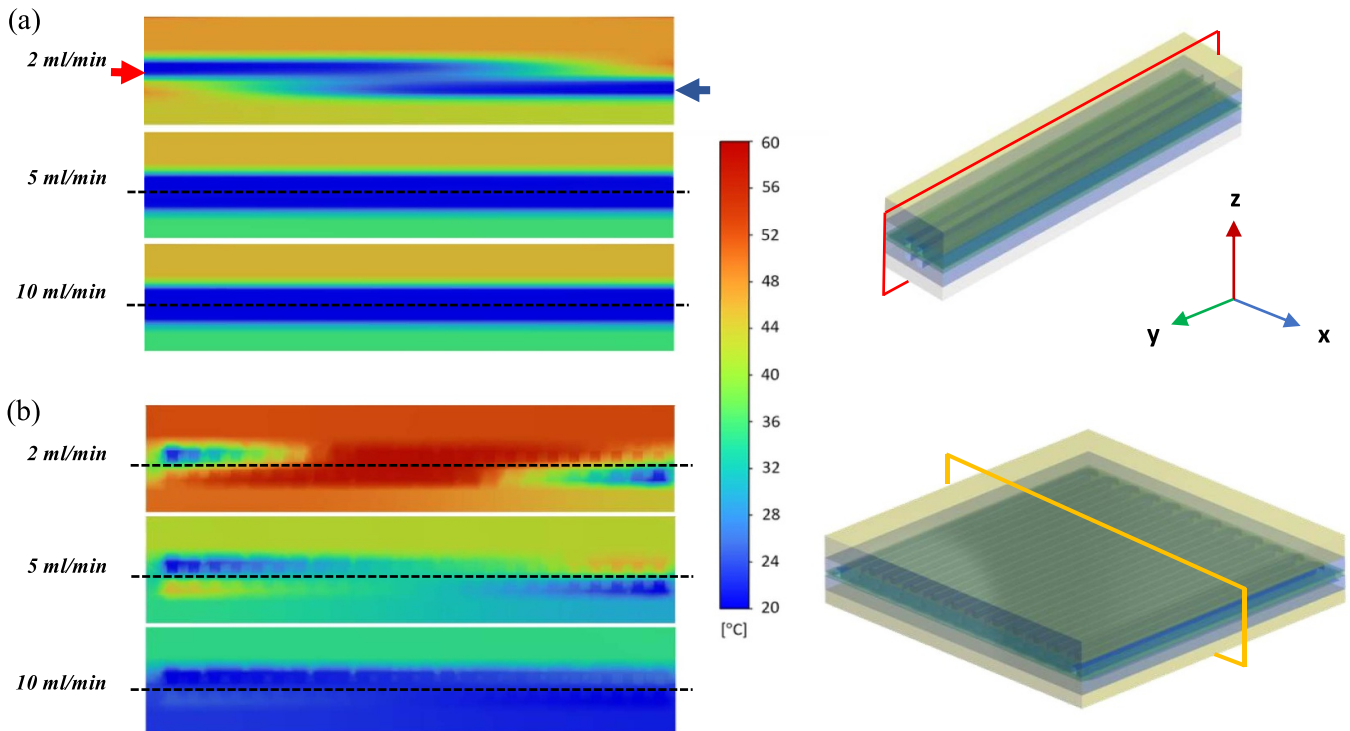


Figure 4. Cross-sectional view of the 2 mm-thick graphite block structure representing the temperature profile for various flow rate, (a) along the straight flow channels (model 1) and (b) perpendicular to the serpentine flow channels' structure (model 2). The centreline highlights the membrane position.

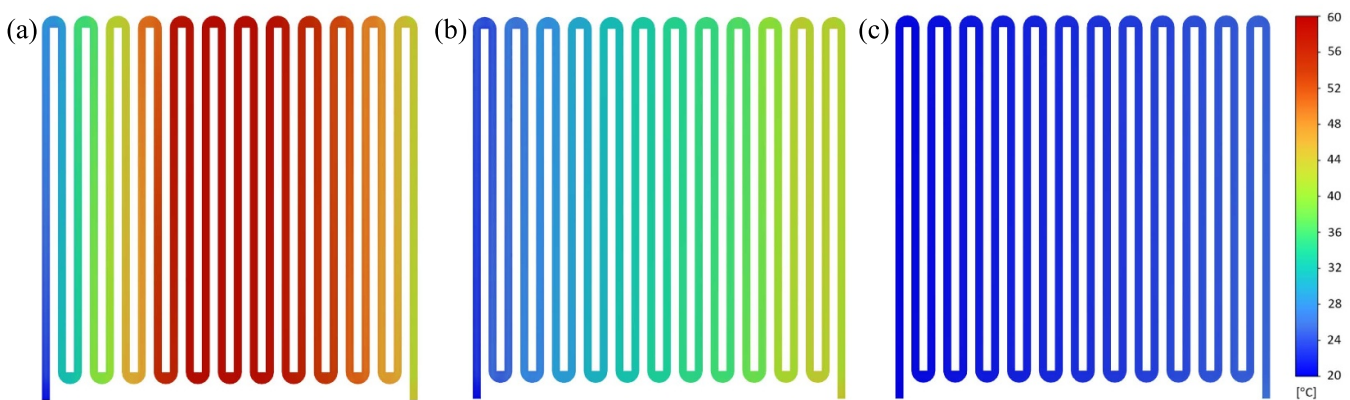


Figure 5. Temperature profile of the top flow channel for the 2 -mm-thick graphite block structure for various flow rate, (a) 2 ml min^{-1} , (b) 5 ml min^{-1} and (c) 10 ml min^{-1} .

it seems that the energy received by the top fluidic electrolyte is transferred to the bottom block through an exchange of heat energy between each fluid. This leads to an increase in the fluid temperature at the end of the bottom flow channel and an indirect cooling of the top fluid. Hence, it is necessary to consider the bottom cell's design aspects, such as the heat exchange through the ion exchange and heat balance between the channels. By highlighting the heat exchange in the middle of the structure, combined with the need for the battery to operate reasonably, the option to control separately the electrolyte flow rates and flow field architectures for top and bottom cells can be considered.

4. Conclusion

In this work, 3D PV-integrated electrochemical flow cells are modeled to investigate the effect of flow channel and graphite thickness variation on the operating temperature of the structure. CFD simulations are also conducted for a range of inlet electrolyte flow rates. Based on the results of this work, to aid further development, we suggest a range of recommendations that can be undertaken:

- A. Thickness: As presented in this work, the simulations conducted have highlighted a better operation when reducing

the graphite thickness to 2 mm and enabling the solar component temperature to decrease. However, considering the serpentine flow channel geometry simulated in Model 2, the results are different, as the fluid exchange system fails to compensate for the amount of energy received by the solar charging component for a low flow rate. Indeed, for each structure considered, we encourage further research to obtain a good combination of structural parameters ensuring thermal stability, a part of which has been investigated in this report.

- B. Electrolyte flow rate: Among the structural parameters, the fluid flow rate must be adapted to favor a low-temperature profile across the PV-integrated flow cell. It has been shown that the overheating of the solar charging component becomes significant at an inlet flow rate below 5 ml min^{-1} , considering the graphite thickness of 2 mm. As considered in section 3.2, a possible flow rate combination can be set up to ensure good battery operation, influencing the temperature profile within the structure.

This combination of thickness and flow rate is subject to a type of electrochemical flow cell system (e.g. type of chemical reaction and PV device material) and the flow channels' geometry considered. The electrolyte flow rate should be high enough in order to ensure heat balance between the electrolyte fluidic field and the incoming heat from the upper part of the structure. In addition, this parameter directly influences the chemical reaction in regulating mass transfer.

Further research can be conducted to analyze the influence of other parameters. For example, the length of the flow channels comprising the serpentine structure can be reduced. This can result in an increase in the solar cell temperature while keeping the temperature of the battery stable even at relatively low flow rates.

5. Future perspectives

The technological readiness of the PV-integrated electrochemical flow cell research area is still at its infancy. Recently, many attempts have been made to realize the PEC or PV charging of a homemade flow cell reactor. However, this view has been pessimistic regarding solar rechargeable electrochemical energy conversion technologies because it has not been difficult to demonstrate its clear advantage over the simple connection between solar PV and RFBs. As predicted in this work, the advantage of a PV-integrated flow cell compared to a simple combination of PV cells and batteries lies in the potential of maximizing the conversion efficiency through active management of external heat. The results of this work will provide a significant stepping stone toward optimizing the flow cell's architectures, which can be expanded to other related electrochemical energy conversion/storage technologies that use

solar energy as a common denominator, such as solar fuel and photocatalysis.

Acknowledgments

The authors acknowledge the Engineering and Physical Sciences Research Council of the UK (EPSRC) for the financial support (EP/X015920/1). D B would especially like to thank Heriot-Watt University for start-up funds.

Conflict of interest

The authors declare that they have no known competing financial interests.

ORCID iDs

Dorian Santander  <https://orcid.org/0009-0004-8149-4934>

Jungmyung Kim  <https://orcid.org/0000-0002-7332-6082>

Dowon Bae  <https://orcid.org/0000-0002-2832-1338>

References

- [1] Bae D, Kanellos G, Faasse G M, Dražević E, Venugopal A and Smith W A 2020 Design principles for efficient photoelectrodes in solar rechargeable redox flow cell applications *Commun. Mater.* **1** 17
- [2] Li W, Fu H C, Zhao Y, He J H and Jin S 2018 14.1% efficient monolithically integrated solar flow battery *Chem* **4** 2644–57
- [3] Li W *et al* 2020 High-performance solar flow battery powered by a perovskite/silicon tandem solar cell *Nat. Mater.* **19** 1326–31
- [4] Khataee A, Azevedo J, Dias P, Ivanou D, Dražević E, Bienten A and Mendes A 2019 Integrated design of hematite and dye-sensitized solar cell for unbiased solar charging of an organic-inorganic redox flow battery *Nano Energy* **62** 832–43
- [5] Ye R, Henkensmeier D, Yoon S J, Huang Z, Kim D K, Chang Z, Kim S and Chen R 2017 Redox flow batteries for energy storage: a technology review *J. Electrochem. Energy Convers. Storage* **15** 010801
- [6] Kamat P V, Karkhanavala M D and Moorthy P N 1979 Temperature effects in photoelectrochemical cells *J. Appl. Phys.* **50** 4228–30
- [7] Tembhumne S, Nandjou F and Haussener S 2019 A thermally synergistic photo-electrochemical hydrogen generator operating under concentrated solar irradiation *Nat. Energy* **4** 399–407
- [8] Dias P, Lopes T, Andrade L and Mendes A 2014 Temperature effect on water splitting using a Si-doped hematite photoanode *J. Power Sources* **272** 567–80
- [9] Lopes T, Dias P, Andrade L and Mendes A 2012 E-MRS/MRS bilateral energy conference innovative technological configurations of photoelectrochemical cells *Energy Proc.* **22** 35–40
- [10] Bae D, Faasse G M and Smith W A 2020 Hidden figures of photo-charging: a thermo-electrochemical approach for solar-rechargeable redox flow cell system *Sustain. Energy Fuels* **4** 2650–5

- [11] Whitley S and Bae D 2021 Perspective—insights into solar-rechargeable redox flow cell design: a practical perspective for lab-scale experiments *J. Electrochem. Soc.* **168** 120517
- [12] Wedege K, Bae D, Smith W A, Mendes A and Bientien A 2018 Solar redox flow batteries with organic redox couples in aqueous electrolytes: a mini-review *J. Phys. Chem. C* **122** 25729–40
- [13] Bae D et al 2015 Back-illuminated Si photocathode: a combined experimental and theoretical study for photocatalytic hydrogen evolution *Energy Environ. Sci.* **8** 650–60
- [14] Leow W Z, Irwan Y M, Asri M, Irwanto M, Amelia A B, Syafiqah Z and Safwati I 2016 Investigation of solar panel performance based on different wind velocity using ANSYS *Indones. J. Electr. Eng. Comput. Sci.* **1** 456–63
- [15] Al-Fetlawi H, Shah A A and Walsh F C 2009 Non-isothermal modelling of the all-vanadium redox flow battery *Electrochim. Acta* **55** 78–89
- [16] Schweiss R, Meiser C, Damjanovic T, Galbiati I and Haak N 2016 SGL GROUP[®] gas diffusion layers for PEM fuel cells, electrolyzers and batteries *SGL Group* pp 1–10
- [17] Kant K, Shukla A, Sharma A and Biwole P H 2016 Heat transfer studies of photovoltaic panel coupled with phase change material *Sol. Energy* **140** 151–61
- [18] Rodriguez A, Adansi R, Enriquez A and Ingram N 2021 ResearchGate Reynolds numbers: The K-epsilon (k-ε) turbulence model vs. laminar model for flow over a circular cylinder multiphase flow project view project scientific machine learning view project (<https://doi.org/10.13140/RG.2.2.14890.13767>)
- [19] Bedeaux D, Flekkøy E G, Hansen A, Kjelstrup S, Måløy K J and Torsaeter O 2020 *Physics of Porous Media* (Frontiers Media SA)
- [20] Gladwell G M L, Huyghe J M, Raats P A C and Cowin S C (eds) 2005 IUTAM symposium on physicochemical and electromechanical interactions in porous media (<https://doi.org/10.1007/1-4020-3865-8>)
- [21] Schweiss R, Meiser C, Damjanovic T, Galbati I and Haak N 2016 SGL Group 2016 (SGL Group) SGL GROUP[®] gas diffusion layers for PEM fuel cells, electrolyzers and batteries
- [22] Lee J, Kim J and Park H 2019 Numerical simulation of the power-based efficiency in vanadium redox flow battery with different serpentine channel size *Int. J. Hydrog. Energy* **44** 29483–92
- [23] da Silva Lopes T, Dias P, Monteiro R, Vilanova A, Ivanou D and Mendes A 2022 A 25 cm² solar redox flow cell: facing the engineering challenges of upscaling *Adv. Energy Mater.* **12** 2102893
- [24] Trovò A, Saccardo A, Giomo M and Guarnieri M 2019 Thermal modeling of industrial-scale vanadium redox flow batteries in high-current operations *J. Power Sources* **424** 204–14
- [25] Chen R, Henkensmeier D, Kim S, Yoon S J, Zinkevich T and Indris S 2018 Improved all-vanadium redox flow batteries using catholyte additive and a cross-linked methylated polybenzimidazole membrane *ACS Appl. Energy Mater.* **1** 6047–55
- [26] Bae D and Bientien A 2022 Take it to the carnot limit: perspectives and thermodynamics of dual-cell electrochemical heat engines *Energy Convers. Manage.* **271** 116315
- [27] Bleeker J, Reichert S, Veerman J and Vermaas D A 2022 Thermo-electrochemical redox flow cycle for continuous conversion of low-grade waste heat to power *Sci. Rep.* **12** 17993
- [28] Kennedy J H and Frese K W 1976 Photo-oxidation of water at barium titanate electrodes *J. Electrochem. Soc.* **123** 1683–6
- [29] Skyllas-Kazacos M, Cao L, Kazacos M, Kausar N and Mousa A 2016 Vanadium electrolyte studies for the vanadium redox battery—a review *ChemSusChem* **9** 1521–43
- [30] Wedege K, Dražević E, Konya D and Bientien A 2016 Organic redox species in aqueous flow batteries: redox potentials, chemical stability and solubility *Sci. Rep.* **6** 39101
- [31] Vermeire F H, Chung Y and Green W H 2022 Predicting solubility limits of organic solutes for a wide range of solvents and temperatures *J. Am. Chem. Soc.* **144** 10785–97
- [32] Tang A, Ting S, Bao J and Skyllas-Kazacos M 2012 Thermal modelling and simulation of the all-vanadium redox flow battery *J. Power Sources* **203** 165–76
- [33] Bae D, Kanellos G, Wedege K, Dražević E, Bientien A and Smith W A 2020 Tailored energy level alignment at MoOX/GaP interface for solar-driven redox flow battery application *J. Chem. Phys.* **152** 124710
- [34] Facchinetti I, Ruffo R, La Mantia F and Brogioli D 2020 Thermally regenerable redox flow battery for exploiting low-temperature heat sources *Cell Rep. Phys. Sci.* **1** 100056
- [35] Ahadi A, Antoun S, Saghir M Z and Swift J 2019 Computational fluid dynamic evaluation of heat transfer enhancement in microchannel solar collectors sustained by alumina nanofluid *Energy Storage* **1** e37